Dielectric response and microwave absorption properties of SiC$_w$/SiC$_f$ composites derived from carbon fiber

Yueshan Mi[1,2], Yang Chen[1,2,*] (iD), Zhanshen Zheng[1,2,*], Yuanliang Li[1,2], Ning Qiao[1,2], and Yuqi Liang[1,2]

[1] Material Science and Engineering School, North China University of Science and Technology, Tangshan 063000, China
[2] Key Laboratory of Inorganic Non-Metallic Materials in Hebei Province, Tangshan 063000, China

ABSTRACT

The SiC$_w$/SiC$_f$ composites composed by SiC whiskers with core–shell structure and SiC fiber with alike-array structure were prepared without growth catalyst, hydrogen silicone oil (H-PSO) as raw material, carbon fiber as the matrix. SiC fibers act as supports for a nanomesh containing interconnected one-dimensional SiC whiskers. The results of studying the absorption properties of the Ku band show that the density of stacking faults decreases and the aspect ratio increases as the heat treatment temperature increases and they jointly affect the dielectric properties of the SiC$_w$/SiC$_f$ composites. The minimum reflection loss of the SiC$_w$/SiC$_f$ composites obtained at 1400 °C can reach − 29.75 dB when the absorber thickness is 3.0 mm, and the effective bandwidth is 2.25 GHz. The polarization relaxation and interfacial polarization in the unique structure improve the microwave absorption properties and broaden the absorption frequency.

1 Introduction

With the development of intelligent technology, electromagnetic wave as the core carrier of information technology is widely used in people's life [1]. However, in both civil and military fields, electromagnetic interference and electromagnetic pollution are inevitably caused, and it has become pollution source with greater harm, which seriously jeopardizes communication and the survival environment [2, 3]. Microwave absorption materials convert incident electromagnetic wave into other forms of energy dissipation through different loss mechanisms, thereby achieving the purpose of absorption electromagnetic wave. Common microwave absorption materials are mainly magnetic materials and carbon materials, such as ferrite [4, 5], carbonyl iron [6], magnetic metal [7], carbon fiber [8], and carbon nanotube [9]. It is difficult for a single lossy material to meet application requirements. Currently, materials with different loss mechanisms are compounded

to improve their loss capability [10–13]. However, ferromagnetism and poor oxidation resistance as well as poor thermal stability make them unable to be used in harsh environments, limiting their applications. Therefore, it is urgent to research the absorption material with steady high-temperature resistance and corrosion resistance. Among them, SiC has attracted everyone's attention due to its high-temperature stability [14–17].

SiC fibers or nanowires are often used to toughen metal or ceramic substrates and have better absorption properties than SiC particles. Duan et al. [18] used aluminum powder as active filler to prepare SiC_f/SiC composites with excellent mechanical and microwave absorption properties. The reflection loss of the composites could reach -56 dB, and the effective bandwidth was 3.4 GHz. Du et al. [19] obtained heterostructural SiC nanowires/SiOC ceramic by pyrolysis of polycarbosilane precursor and the minimum reflection loss reached − 10 dB at 13 GHz. As high-temperature microwave absorption materials, one-dimensional SiC material has attracted the attention of more and more researchers. However, in many cases, the yield of SiC nanowires is low, the uniformity is poor, and there are catalyst residues. A single SiC material has limited microwave absorption performance due to its poor dielectric loss, but the second phase substance such as composite magnetic particles in the SiC material have adverse effects on its high-temperature performance. The main research here is composite material composed of single SiC, and it is expected that the multiple structure and internal defects of SiC improve its absorption performance while ensuring its high-temperature stability.

In this study, SiC_w/SiC_f composites based on in situ growth of SiC whisker on carbon fibers were obtained by organic polymer conversion with low-cost hydrogen silicone oil (H-PSO) as precursor, carbon fibers as matrix, without growth catalyst. The composites with unique structure were composed by SiC whiskers (SiC_w) and SiC fiber (SiC_f) with fibrillar structure inherited from carbon fiber. The SiC_w grown by this method has good quality and no catalyst pollution. Furthermore, the fibrillar structure of SiC_f derived from carbon fiber, with the "alike-array structure" that improved the electromagnetic attenuation ability, broadened the absorption frequency.

2 Experimental

2.1 Preparation of SiC_w/SiC_f composites

Carbon fiber (Carbon Fiber Engineering Research Center, Faculty of Materials Science, Shandong University) was used as matrix preparation of SiC_w/SiC_f composites, and it was heated to 1500 °C for 2 h in argon (99.999%) atmosphere to remove surface organics. H-PSO (CH_3–$(SiO)_n$–Si–H, Jinan Guobang Chemical Co. Ltd., China) was precursor, and chloroplatinic acid ($H_2PtCl_6 \cdot 6H_2O$; Jinan Luli Chemical Co. Ltd., China) was cross-linked catalyst. Two drops of chloroplatinic acid ethanol solution were added (1 wt%) to 20 ml H-PSO, stirred with magnetic stirrer for 20 min, and kept at 120 °C. The cross-linked product was powdered by a sealing mill. As embedded powders, they were placed in crucibles to embed carbon fibers, and SiC_w/SiC_f composites was grown at 1400 °C, 1500 °C, and 1600 °C for 2 h in tubular atmosphere furnace under argon atmosphere, and the heating rate increase by 4 °C per min at 800 °C, and 2 °C per minute above 800 °C. Finally, it was decarburized in chamber furnace at 800 °C for 4 h. The sample prepared at different temperatures was marked as SiC-1400, SiC-1500 and SiC-1600.

2.2 Characterization

The crystal phase and composition of the SiC_w/SiC_f composites were identified by X-ray diffraction (XRD, D/MAX2500PC, 4°/min). Scanning electron microscopy (SEM, FEI Scios) and transmission electron microscopy (TEM, JEOL-2800) were used to characterize the morphology and structure. The Nano Measurer software was used to measure and calculate the diameter and the aspect ratio distribution of SiC_w was shown in SEM images for measure, and the average was recorded. The sample and paraffin were mixed at a mass ratio of 1:3, and then pressed this into a toroidal shape with a 3 mm inner diameter and 7 mm outer diameter. The vector network analyzer is used to measure the electromagnetic parameters (ε', ε'', μ', μ'') in the Ku band, and the reflection loss (RL) was calculated by the transmission line theory [20–22]:

$$Z_{in} = \sqrt{\frac{\mu_r}{\varepsilon_r}} \tanh\left[j\frac{2\pi fd}{c}\sqrt{\mu_r\varepsilon_r}\right] \tag{1}$$

$$R(dB) = 20\lg\left|\frac{Z_{in} - 1}{Z_{in} + 1}\right| \tag{2}$$

where c is the velocity of light, f is the frequency of electromagnetic wave, d is the thickness of the absorber material, $\mu_r(\mu_r = \mu_r' - \mu_r'')$ is the complex permittivity of the materials, $\varepsilon_r(\varepsilon_r = \varepsilon_r' - \varepsilon_r'')$ is the complex permeability of the materials, and Z_{in} is the normalized input wave impedance incident on the material interface in free space.

3 Results and discussion

3.1 Morphology and structure of the SiC_w/ SiC_f composites

Figure 1a shows the XRD pattern of the SiC_w/SiC_f composites prepared at 1500 °C. It shows three distinct characteristic peaks at 35.6°, 60.0°, and 71.7°, corresponding to the (111), (220), and (311) crystal planes of 3C-SiC (JCPSD file: 65-0360). In addition, the peak at 33.6° indicates high-density stacking

faults in the SiC_w [23]. Further analysis of XRD shows that in the SiC_w/SiC_f composite, SiC has a cubic phase structure and the SiO_2 content is 3.92% (as shown in Table 1). As shown in Fig. 1b–d, the SiC_w/ SiC_f composites contain SiC_w and SiC_f. Although there is no growth catalyst, the yield of SiC_w obtained in this way is not lower than other methods. EDS analysis was performed on the head and stem of the whiskers as shown in Fig. S1. The whiskers were mainly composed of Si and C elements, with a small amount of O element. This also proves that chloroplatinic acid has not become a catalyst for whisker growth. The diameter of SiC_w is generally hundreds of nanometers, and evenly covers the matrix. As shown in Fig. 2a, SiC_w has core–shell structure with outer shell of about 10 nm. Given that the peak belongs to the diffraction peak of amorphous SiO_2 at 22° in Fig. 1a, the outer layer of SiC_w is amorphous SiO_2. Due to the high-density stacking faults in the material, there are also a large number of dark stripes in the Fig. 2a (as shown in the red circle) [24]. In addition, SiC_f retains the "alike-array structure", which "inherits" the fibrillar structure of carbon fiber
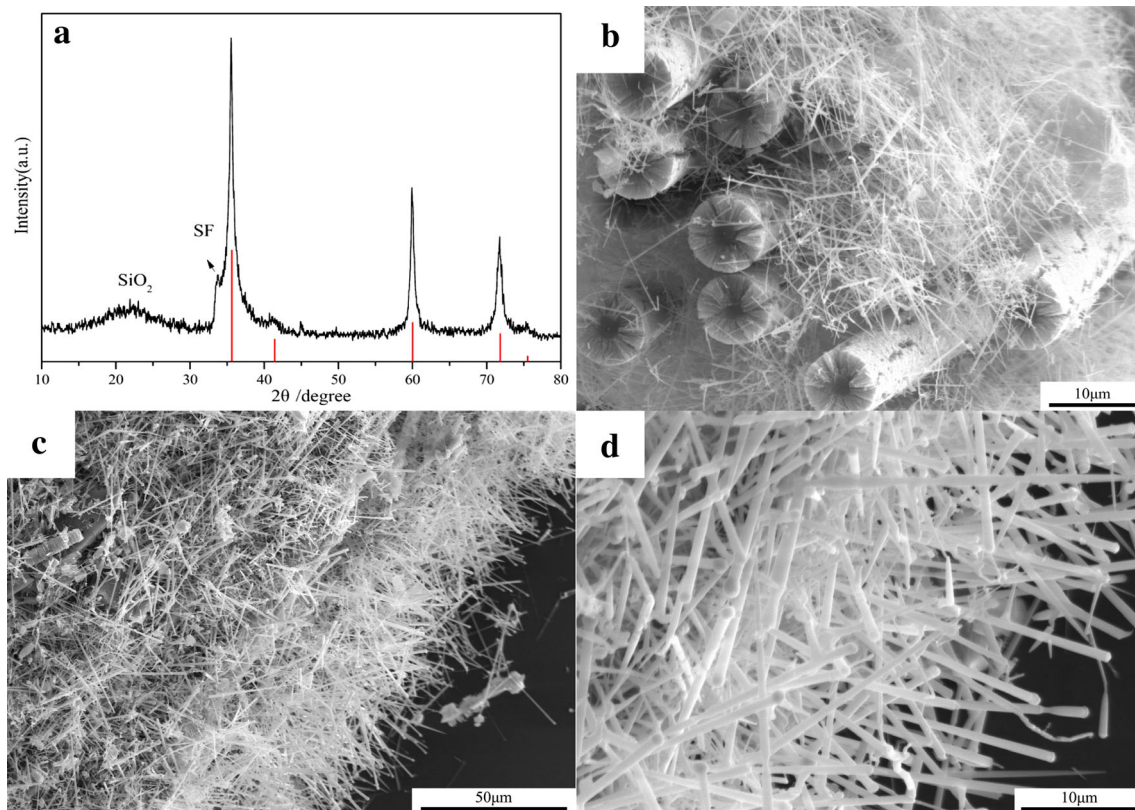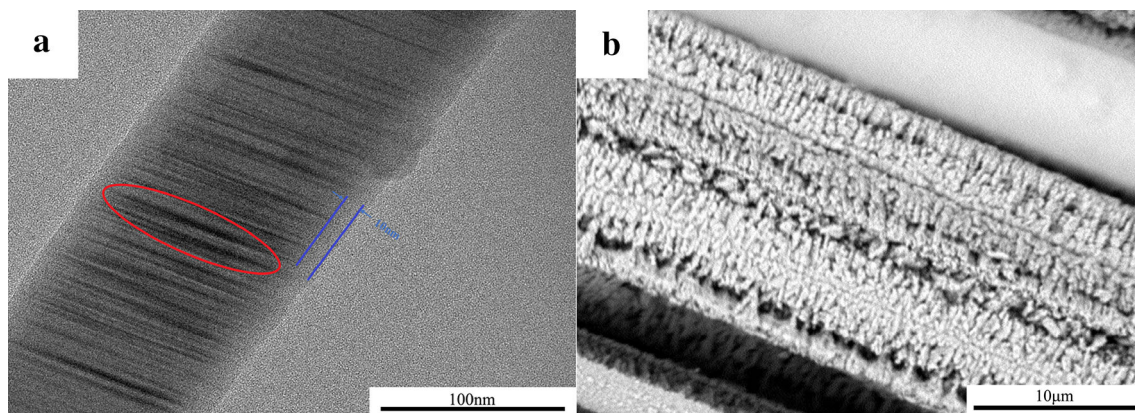

Fig. 1 Morphology and structure of the SiC_w/SiC_f composites prepared at 1500 °C. (**a** XRD pattern; **b**–**d** SEM image of SiC_w/SiC_f composites)

Table 1 Crystal structure parameters of SiC composite

Parameters	3C–SiC	SiO$_2$
R_w(%)	5.811	
Proportion(%)	96.08	3.92
Space group	F-43 m	P3221
a(Å)	4.3618	4.9317
b(Å)	4.3618	4.9317
c(Å)	4.3618	5.3692
Alpha(°)	90	90
Beta(°)	90	90
Gamma(°)	90	120

[25] (as shown in Fig. 2b). That is, when carbon fiber was used as matrix during the growth of SiC$_w$, SiC replaced the position of C and retained the fibrillar structure of the carbon fiber and the expected "alike-array structure" of SiC$_f$ is successfully prepared. In addition, the SiC$_f$ becomes the support of the nano-mesh containing interconnected one-dimensional SiC$_w$ as show in Fig. 1b, c. However, because the SiC radius is larger than the radius of C, the SiC$_f$ cracks. This structure has greater interface polarization than ordinary SiC$_f$, and also increases the scattering and multiple reflections of incident wave, which is conducive to electromagnetic loss. In addition, the presence of cracks in the fibrillar structure improves electromagnetic resonance loss and impedance matching, which is beneficial to broaden the absorption band [26].
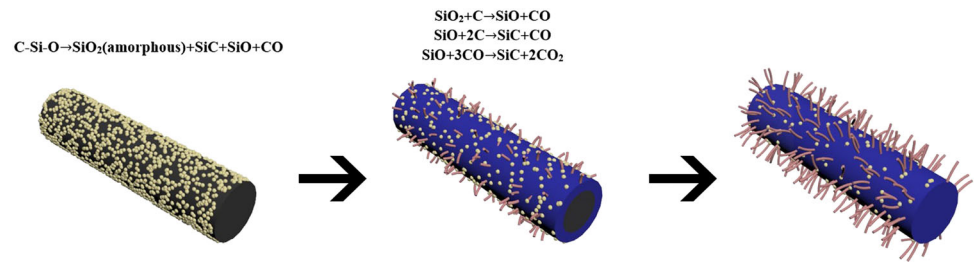
3.2 Growth mechanism of the SiC$_w$/SiC$_f$ composites

The formation process of the SiC$_w$/SiC$_f$ composite is shown in Fig. 3. The SiOC ceramic was formed by cross-linked of H-PSO. At high temperature, SiOC ceramic could generate SiC and silicon or carbon-containing gas due to phase separation. At the same time, a part of SiO$_2$ was reduced by carbon around, and the generated SiO diffused to the surface of the carbon fiber and reacted with it to form SiC. As the reaction continued, the new SiO continued to react with the surrounding C and CO, and the generated SiC deposited along the lowest energy crystal plane to form SiC$_w$ [27]. Molten SiO$_2$ covered the SiC crystal nucleus, and gaseous SiO and CO penetrated the silicon oxide film and continued to participate in the reaction at higher temperatures. After the system temperature was reduced, unreacted SiO$_2$ covered the surface of the SiC$_w$ to form SiC$_w$ with core–shell structure (SiC@SiO$_2$). The presence of SiO$_2$ will benefit the material's impedance matching ability due to its good electromagnetic wave permeability. Previous studies have shown that surface SiO$_2$ is consumed less and less as temperatures rise [28], which will certainly affect the absorption property of the material. In addition, as the whisker grows, carbon fiber as a carbon source participated in the reaction, and SiC replaced C to form SiC$_f$, but due to the larger radius of SiC, a slight cracking occurred, as show in Fig. 1b.

3.3 Dielectric response of the SiC$_w$/SiC$_f$ composites

As far as we know, the heat treatment temperature is an important factor affecting the growth of crystals,

Fig. 2 Morphology of the SiC$_w$ and SiC$_f$. (**a** TEM image of SiC$_w$; **b** SEM image of SiC$_f$ with alike-array structure)

Fig. 3 Schematic diagram of the SiC$_w$/SiC$_f$ composites

because it affects the amount of gas generated by pyrolysis and provides energy fluctuation for the nucleation and growth of crystals [27], which in turn affects the microwave absorption properties of the material. Therefore, three different heat treatment temperatures were selected to prepare the SiC$_w$/SiC$_f$ composite to study its absorption properties.

SiC as non-magnetic material, the values of μ_r'' (imaginary part of permeability) and μ_r' (real part of permeability) is considered to be 0 and 1, respectively [29]. So the investigation mainly focuses on the complex permittivity. In general, the relative complex permittivity is expressed by complex number ($\varepsilon_r = \varepsilon_r' - \varepsilon_r''$), where the real part ε_r' represents the ability to store energy, and the imaginary part ε_r'' represents the conductivity and dielectric loss [30]. As displayed in Fig. 4, the samples have dielectric resonance peak, which the polarization cannot respond to changes in higher frequency electric fields. The imaginary part of the permittivity decreases first and then increases with increasing temperature. The imaginary part of permittivity of SiC-1600 is larger and the peak value is shifted to higher frequency. However, SiC-1500 has the lowest
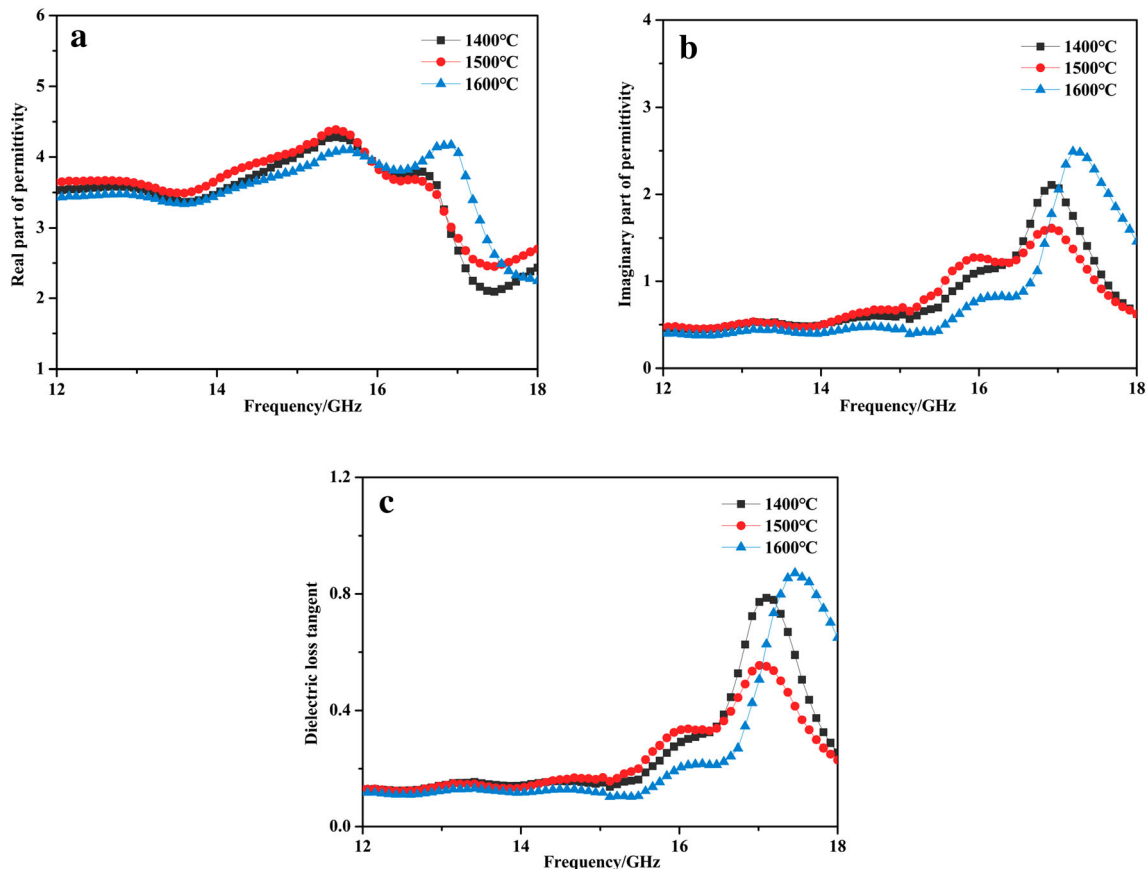

Fig. 4 Dielectric response of SiC$_w$/SiC$_f$ composites prepared at different temperatures. (**a** real part; **b** imaginary part; **c** dielectric loss tangent)
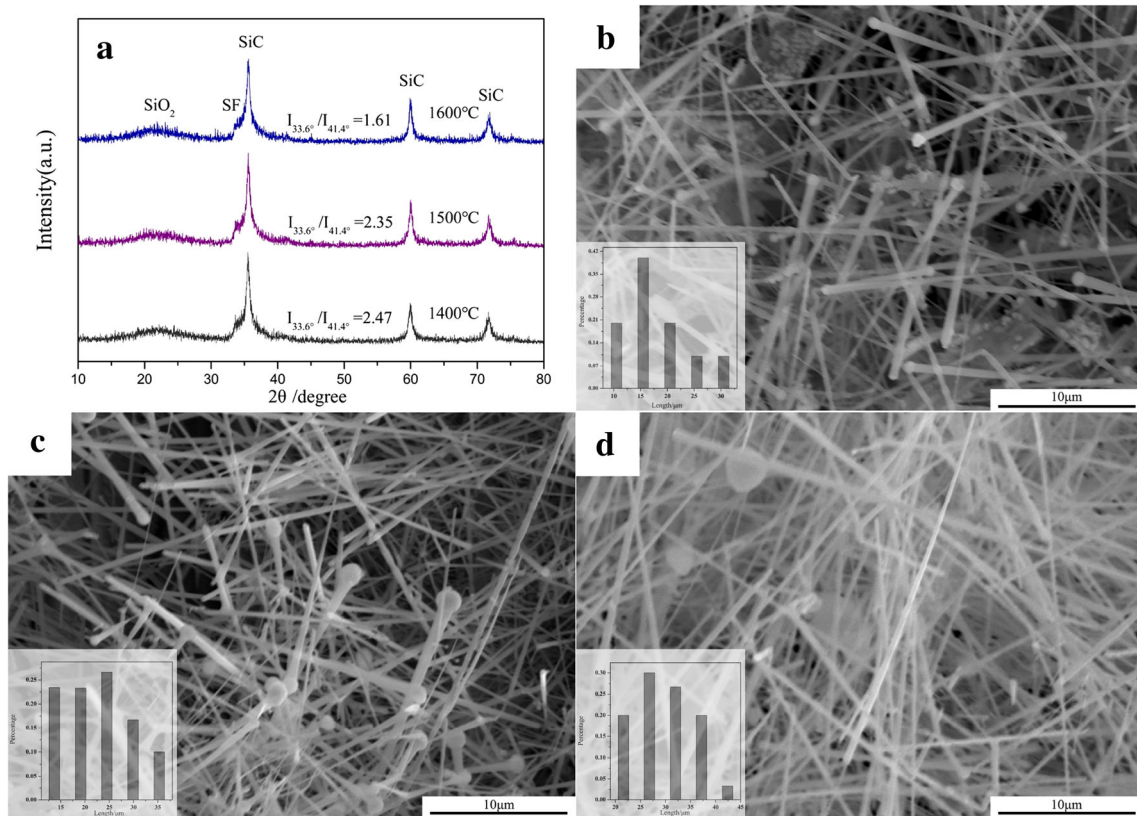
Fig. 5 XRD images and SEM image of the SiC_w/SiC_f composites at different temperatures. (**a** XRD image; SEM image of **b** 1400 °C; **c** 1500 °C; **d** 1600 °C)

imaginary part of permittivity. Figure 4c shows the variation of the dielectric loss tangent of SiC_w/SiC_f composite with frequency, which is consistent with the trend of the imaginary part of permittivity.

From the above we can see that the SiC_w/SiC_f composite material is composed of SiC_w and SiC_f. However, temperature has little effect on SiC_f because of the high-temperature structure that comes from carbon fiber. Therefore SiC_w is the main reason that affects the phase structure and dielectric properties of composite materials.

In XRD pattern(as shown in Fig. 5a), the peak intensity ratios of the diffraction peaks at 33.6° and 41.4° ($I_{33.6°}/I_{41.4°}$) are used to measure the content of stacking faults in the SiC lattice. A larger ratio means more stacking faults [31]. Because temperature has little effect on the phase structure of SiC_f, the $I_{33.6°}/I_{41.4°}$ values in Fig. 5a can be used to characterize the stacking faults of the one-dimensional SiC_w. The $I_{33.6°}/I_{41.4°}$ values of SiC_w prepared at 1400 °C, 1500 °C and 1600 °C are 2.47, 2.35 and 1.61, respectively. It shows that higher temperature is conducive to the reduction of stacking faults density. In general, SiC_w

forms stacking faults in order to reduce the energy required for growth. The higher temperature provides more energy, and the driving force for whisker growth increases, that is not need more stacking faults to promote growth. Therefore, as the temperature increases, the stacking faults density decreases. Kuang et al. [32] found that the charge separation at the heterostructure interface of stacking faults resulted in a large number of interface dipoles, which led to an increase in dipole polarization. This is why the dielectric loss of SiC-1400 is higher. Figure 5a shows that the stacking fault density of SiC-1600 is the lowest, but it still shows higher dielectric loss capacity (Fig. 4c), which indicates that there are other factors affecting the dielectric response besides stacking fault.

Figure 5b–d shows SEM images of SiC_w in the composites obtained at different temperatures. At low temperature, some whiskers have molten droplets on their heads due to the low melting point of SiO_2. As the heat treatment temperature increases, the molten SiO_2 continues to be reacted, the diameter of the SiC_w decreases and the length increases. The

main reason is that the concentration of the reaction gas increases at higher temperature. Higher reaction gas concentration leads to increase of the nucleation point, which leads to increase in whisker production, thereby reduces the lateral growth of SiC_w and increases the length. As the reaction continues, the head SiO_2 is continuously converted to SiC, resulting in an increase in length. The length increases significantly, and it is easier to overlap each other to form conductive network [33]. As the distance between the whiskers decreases, the probability of electron jump transfer increases, which promotes the dielectric loss. That is why, despite the absence of high stacking faults, SiC-1600 still has higher dielectric loss capacity, which is related to the electron transfer caused by the high aspect ratio. It could also be the reason why the loss peak of SiC-1600 shifts to high frequency.

To sum up, although both SiC-1400 and SiC-1600 have higher dielectric loss, the main contribution mechanism is different, which is the high stacking fault density (SiC-1400) and high aspect ratio (SiC-1600), respectively. In addition, the polarization at the point defects on the SiC_w and the "alike-array structure" of SiC_f also lead to an increase in dielectric loss under the action of external electromagnetic fields.

3.4 Microwave absorption properties of the SiC_w/SiC_f composites

To evaluate the microwave absorption properties of the SiC_w/SiC_f composites, the reflection loss of SiC-1400, SiC-1500 and SiC-1600 with different thickness were calculated, as shown in Fig. 6a–c. The reflection loss of SiC-1400 reaches $-$ 29.75 dB at 17.37 GHz when the absorber thickness is 3.0 mm, and the effective bandwidth is 2.25 GHz. The lowest reflection losses of SiC-1500 and SiC-1600 are $-$ 22.28 dB and $-$ 22.73 dB, respectively, which are not much different (as shown in Fig. 6d). Although the stacking fault density of SiC-1500 is higher than that of SiC-1600, it has been confirmed above that the high aspect ratio of SiC-1600 promotes electron transitions, thus showing higher dielectric loss derived from electron displacement polarization. The SiC_w/SiC_f composites prepared by this method are composed of SiC_w and SiC_f with a large specific surface area, which increases the interface polarization of the materials and improves the absorption performance.

The microwave absorption ability of the SiC_w/SiC_f composites is determined by dielectric loss and impedance matching [34]. To further study the microwave absorption mechanism, the attenuation constant α and impedance Z_{in} need to be studied. In general, the closer the impedance of the absorption material is to the impedance of free space, the easier it is for electromagnetic waves to enter the material. The attenuation constant α represents the attenuation ability of the material to EM waves. The attenuation constant α and impedance Z_{in} are calculated according to the following formula.

$$\alpha = \frac{\pi f \sqrt{2\mu'\varepsilon'}}{c} \sqrt{\frac{\varepsilon''\mu''}{\varepsilon'\mu'} - 1 + \sqrt{\left(\frac{\varepsilon''\mu''}{\varepsilon'\mu'}\right)^2 + \left(\frac{\varepsilon''}{\varepsilon'}\right)^2 + \left(\frac{\mu''}{\mu'}\right)^2 + 1}} \tag{3}$$

$$|Z_{in}| = \left| \sqrt{\frac{\mu_r}{\varepsilon_r}} \tanh\left[j\frac{2\pi fd\sqrt{\mu_r\varepsilon_r}}{c}\right] \right| \tag{4}$$

As displayed in Fig. 7a, SiC-1600 has higher α value, suggesting that the superior attenuation ability of SiC-1600 for the incident EM waves. Similarly, the impedance of SiC-1600 is farthest away from 1, and EM waves are most likely to enter the material. The absorption performance of the material is determined by the attenuation ability and impedance matching. Although the attenuation ability of SiC-1600 is better than that SiC-1400, the absorption performance is still worse than that SiC-1400. SiC-1400 shows higher attenuation ability due to higher stacking faults, while better impedance matching due to more SiO_2 on the surface of SiC_w.

According to Debye theory, the relationship between ε' and ε'' is

$$\left(\varepsilon' - \frac{\varepsilon_s + \varepsilon_\infty}{2}\right)^2 + \varepsilon''^2 = \left(\frac{\varepsilon_s - \varepsilon_\infty}{2}\right)^2 \tag{5}$$

where ε_s is the static permittivity, ε_∞ is the relative dielectric permittivity at infinite high frequency. The graph of ε'–ε'' is called the Cole–Cole curve [35]. The presence of semicircles in Cole–Cole curve represents that the samples have certain relaxation polarization ability. The disordered curve in Fig. 8a–c indicates that there are several semicircles in the curve, which indicates that they have various dielectric relaxation processes under electromagnetic fields. There are several reasons for this. Firstly, the internal free charge move under the action of an external electric field, which is trapped and accumulated at the stacking fault of SiC_w or the "alike-array structure" of SiC_f, resulting in accumulation of charge, making the
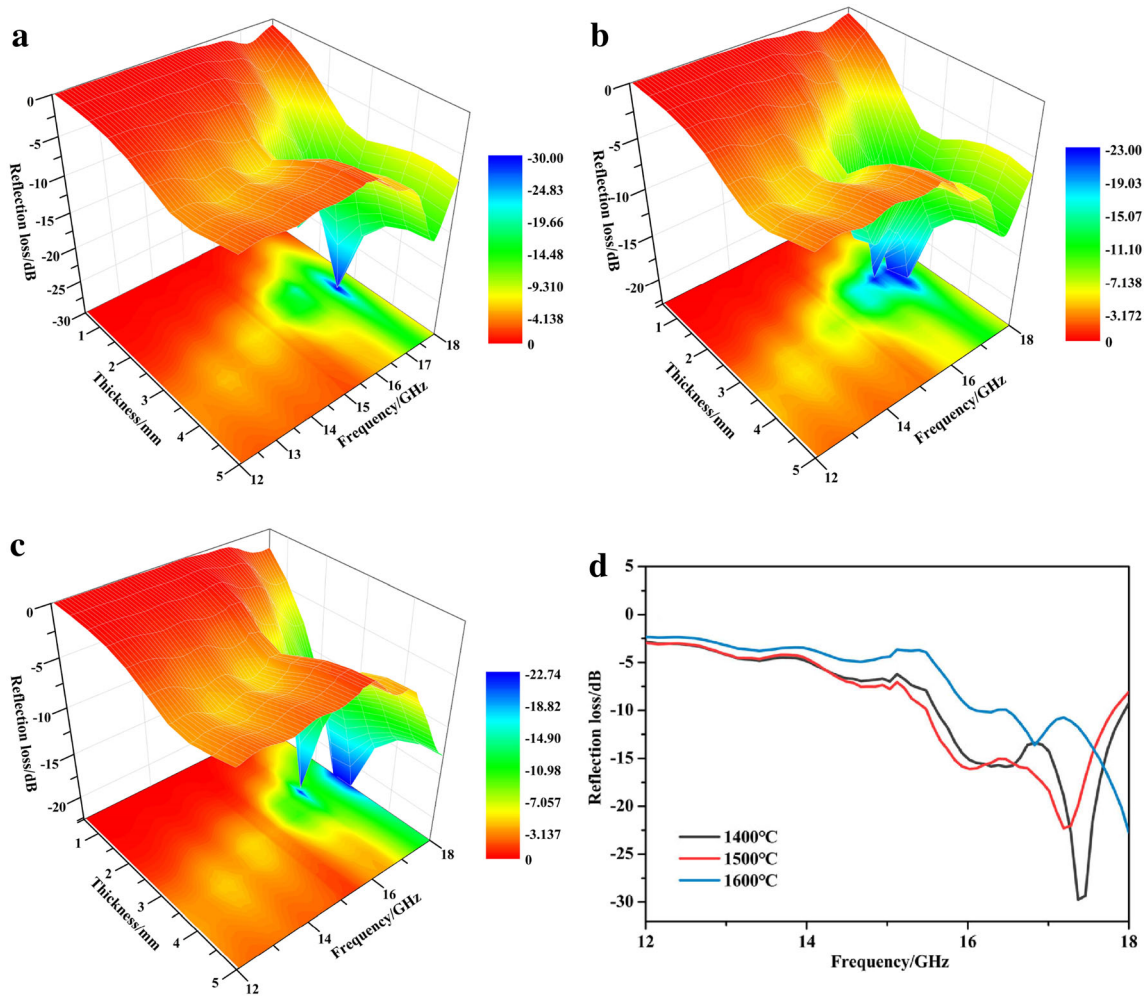
Fig. 6 Reflection loss at different thickness of the SiC$_w$/SiC$_f$ composites at different temperatures. (**a** 1400 °C; **b** 1500 °C; **c** 1600 °C; **d** Reflective loss of 5 mm thickness)
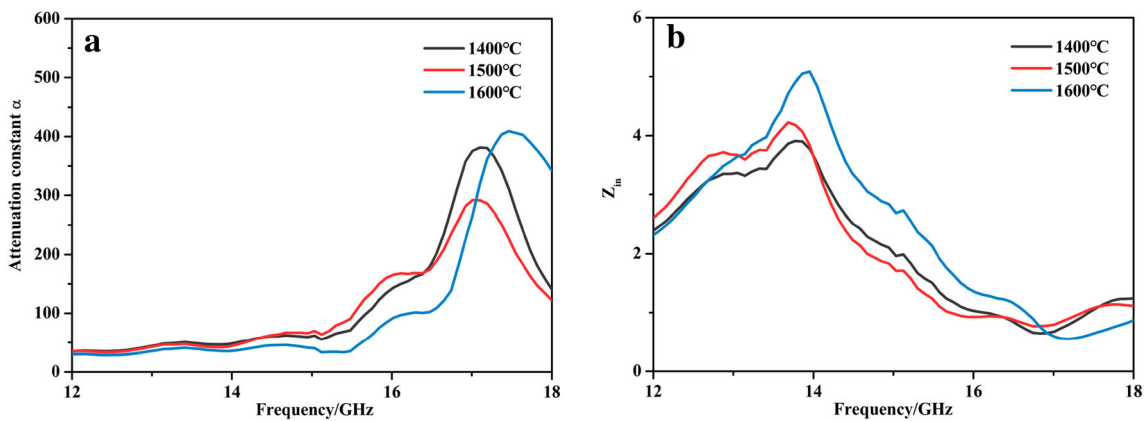

Fig. 7 Attenuation constant and impedance of SiC$_w$/SiC$_f$ composites. (**a** Attenuation constant; **b** Impedance)

charge distribution uneven and dipole polarization more obvious. Secondly, the SiC$_w$ has higher aspect ratio and forms 3D network, thus electron transitions

is more likely to occur between the whiskers, which leads to large electron displacement polarization and increases the multiple reflection of electromagnetic
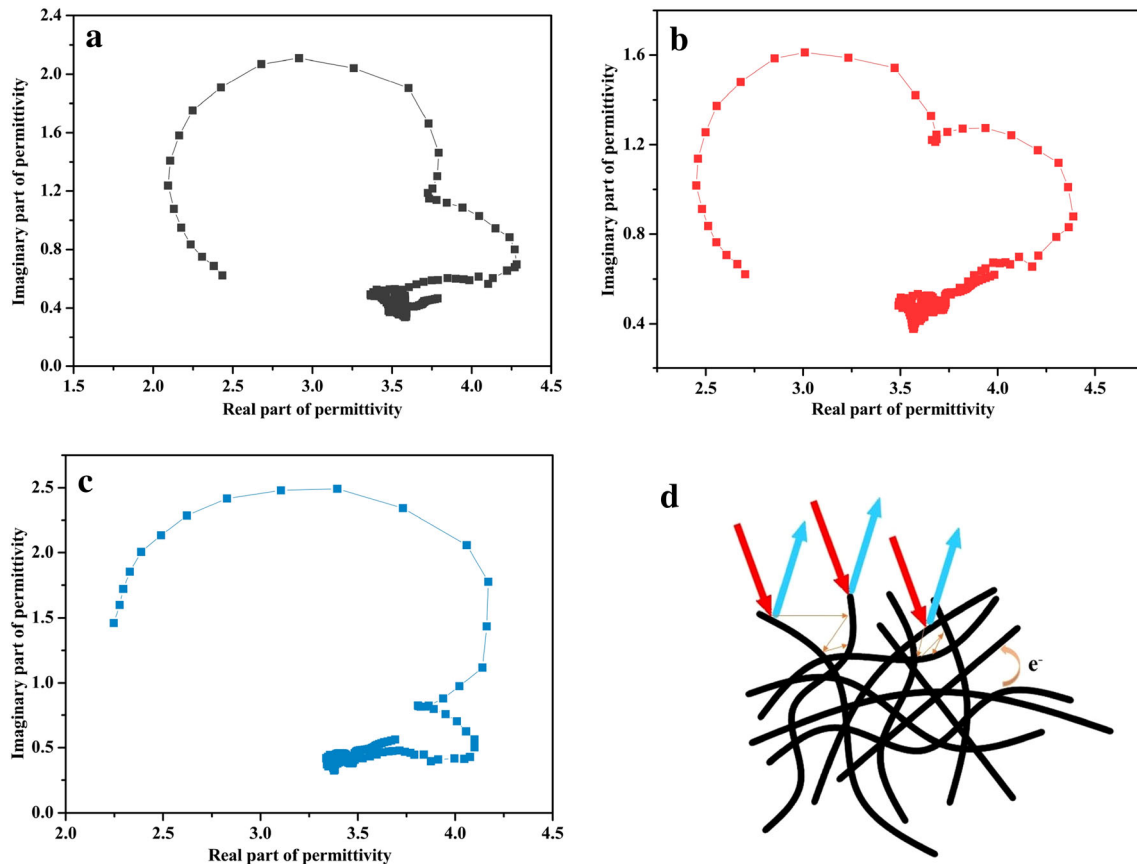
Fig. 8 Cole–cole curve and the multiple reflection mechanism of SiC$_w$/SiC$_f$ composite. (**a** 1400 °C; **b** 1500 °C; **c** 1600 °C; **d** multiple reflection mechanism)

wave, as shown in Fig. 8d. Additionally, the high specific surface area of SiC$_w$/SiC$_f$ composites also promotes the interface polarization. Overall, these relaxations corresponding to Cole–Cole curve should be attributed to the rich interfacial polarization, electric dipole polarization, and trapping center polarization in the unique structure of SiC$_w$/SiC$_f$ composites, which is conducive to the improvement of dielectric loss, thereby improve the absorption performance.

4 Conclusion

The SiC$_w$/SiC$_f$ composites were experimentally prepared based on in situ growth of SiC whisker on carbon fibers. The materials were composed by SiC$_w$ with core–shell structure (SiC@SiO$_2$) and SiC$_f$ with the "alike-array structure" inherited from carbon fiber, which was prepared by hydrogen silicone oil as the raw material and carbon fiber as the matrix

without growth catalyst. Among them, the SiC$_w$ have good uniformity, and the SiC$_f$ retain the fibril structure of carbon fiber. As the heat treatment temperature increases, the density of stacking defects of the SiC$_w$ decreases and the aspect ratio increases. The dielectric properties of SiC$_w$/SiC$_f$ composites are attributed to the combined effect of stacking faults and aspect ratio of SiC$_w$. The reduction of stacking faults leads to reduction of dipole polarization, which reduces the dielectric loss, but the increase of the aspect ratio leads to increase of electron displacement polarization, which increases the dielectric loss. The presence of SiO$_2$ coated on SiC$_w$ is helpful to improve the impedance matching of the material. In addition, interfacial polarization and relaxation polarization are also conducive to the improvement of absorption performance. The whiskers grown at different heat treatment temperatures may exhibit different loss mechanisms. The minimum reflection loss of the SiC$_w$/SiC$_f$ composites obtained at 1400 °C reach −

29.75 dB, and the effective bandwidth is 2.25 GHz in 3 mm thickness.

References

1. X.Y. Yuan, L.F. Cheng, L. Kong et al., Preparation of titanium carbide whiskers for application in electromagnetic wave absorption. J. Alloys Compd. **596**, 132–139 (2014)

2. A. Siriwitpreecha, P. Rattanadecho, T. Wessapan, The influence of wave propagation mode on specific absorption rate and heat transfer in human body exposed to electromagnetic wave. Int. J. Heat Mass Transf. **65**, 423–434 (2013)

3. P. Bandara, O.C. David, Planetary electromagnetic pollution: it is time to assess its impact. Lancet Planet. Health **2**, e512–e514 (2018)

4. E. Handoko, I. Sugihartono, S. Budi et al., The effect of thickness on microwave absorption properties of barium ferrite powder. J. Phys. Conf. Ser. **1080**, 1–7 (2018)

5. A.N. Hapishah, M. Msyazwan, M.H. Hamidon, Synthesis and characterization of magnetic and microwave absorption properties in polycrystalline cobalt zinc ferrite ($Co_{0.5}Zn_{0.5}$-Fe_2O_4) composite. J. Mater. Sci-Mater. El. **29**, 20573–20579 (2018)

6. Y.Y. Zhou, H. Xie, W.C. Zhou et al., Enhanced antioxidation and microwave absorption properties of SiO_2-coated flaky carbonyl iron particles. J. Magn. Magn. Mater. **446**, 143–149 (2018)

7. X.G. Su, J. Wang, X.X. Zhang et al., Design of hierarchical 1D–2D $NiCo_2O_4$ as high-performance microwave absorber with strong loss and wide absorption frequency. J. Mater. Sci-Mater. El. **30**, 16287–16297 (2019)

8. X.L. Chen, X.W. Wang, L.D. Li et al., Preparation and microwave absorption properties of nickel-coated carbon fiber with polyaniline via in situ polymerization. J. Mater. Sci-Mater. El. **27**, 5607–5612 (2016)

9. W.L. Pan, M. He, X.H. Bu et al., Microwave absorption and infrared emissivity of helical polyacetylene@multiwalled carbon nanotubes composites. J. Mater. Sci-Mater. El. **28**, 8601–8610 (2017)

10. S.V. Truknanov, A.V. Truknanov, V.G. Kostishin et al., Magnetic and absorption properties of M-type substituted hexaferrites $BaFe_{12−x}Ga_xO_{19}$ ($0.1 < x < 12$). J. Exp. Theor. Phys. **123**, 461–469 (2016)

11. L.Y. Matzui, A.V. Trukhanov, O.S. Yakovenko et al., Functional magnetic composites based on hexaferrites: correlation of the composition, magnetic and high-frequency properties. Nanomaterials **9**, 1720 (2019)

12. O.S. Yakovenko, L.Y. Matzui, L.L. Vovchenko et al., Electrophysical properties of epoxy-based composites with graphite nanoplatelets and magnetically aligned magnetite. Mol. Cryst. Liq. Cryst. **661**, 68–80 (2018)

13. D.A. Vinnik, D.S. Klygach, V.E. Zhivulin et al., Electromagnetic properties of $BaFe_{12}O_{19}$:Ti at centimeter wavelengths. J. Alloys Compd. **755**, 177–183 (2018)

14. Y.C. Wang, P. Xiao, W. Zhou et al., Microstructures, dielectric response and microwave absorption properties of polycarbosilane derived SiC powders. Ceram. Int. **4**, 3606–3613 (2018)

15. X.L. Ye, Z.F. Chen, M. Li et al., Microstructure and microwave absorption properties variation of SiC/C foam at different elevated-temperature heat treatment. ACS Sustain. Chem. Eng. **7**, 18395–18404 (2019)

16. S. Dong, X.H. Zhang, D.Y. Zhang et al., Strong effect of atmosphere on the microstructure and microwave absorption properties of porous SiC ceramics. J. Eur. Ceram. Soc. **1**, 29–39 (2018)

17. T. Han, R.Y. Luo, G.Y. Cui et al., Effect of SiC whiskers on the high-temperature microwave absorption properties of SiC_f/SiC composites. J. Eur. Ceram. Soc. **5**, 1743–1756 (2019)

18. S.C. Duan, D.M. Zhu, J. Dong et al., Enhanced mechanical and microwave absorptionproperties of SiC_f/SiC composite using aluminum powder as active filler. J. Alloys Compd. **790**, 58–69 (2019)

19. B. Du, C. He, A. Shui et al., Microwave-absorption properties of heterostructural SiC whiskers/SiOC ceramic derived from polysiloxane. Ceram. Int. **45**, 1208–1214 (2019)

20. L.W. Yan, C.Q. Hong, B.Q. Sun et al., In situ growth of core−sheath heterostructural SiC whisker arrays on carbon fibers and enhanced electromagnetic wave absorption properties. ACS. Appl. Mater. Interfaces **7**, 6320–6331 (2017)

21. A.V. Trukhanov, K.A. Astapovich, M.A. Almessiere et al., Pecularities of the magnetic structure and microwave properties in $Ba(Fe_{1−x}Sc_x)_{12}O_{19}$ ($x < 0.1$) hexaferrites. J. Alloys Compd. **822**, 153575 (2020)

22. M.A. Almessiere, Y. Slimani, H. Güngüneş et al., Impact of Eu^{3+} ion substitution on structural, magnetic and microwave

traits of Ni–Cu–Zn spinel ferrites. Ceram. Int. **46**, 11124–11131 (2020)

23. Y. Luo, S.L. Zheng, S.H. Ma et al., Novel two-step process for synthesising β-SiC whiskers from coal fly ash and water glass. Ceram. Int. **44**, 10585–10595 (2018)

24. H.Y. Zhang, Y.J. Xu, J.G. Zhou et al., Stacking fault and unoccupied densities of state dependence of electromagnetic wave absorption in SiC whiskers. J. Mater. Chem. C **3**, 4416–4423 (2015)

25. C. Kunzmann, J. Moosburger-Will, S. Horn, High-resolution imaging of the nanostructured surface of polyacrylonitrile-based fibers. J. Mater. Sci. **51**, 9638–9648 (2016)

26. H.L. Xu, X.W. Yin, M.H. Li et al., Ultralight cellular foam from cellulose nanofiber/carbon nanotube self-assemblies for ultrabroad-band microwave absorption. ACS Appl. Mater. Interfaces **25**, 22628–22636 (2019)

27. Y.S. Mi, Y. Chen, Z.S. Zheng et al., New discoveries in the growth of SiC whiskers derived from hydrogen silicone oil. J. Cryst. Growth **543**, 125711 (2020)

28. Y. Chen, C.G. Wang, B. Zhu et al., Growth of SiC whiskers from hydrogen silicone oil. J. Cryst. Growth **357**, 42–47 (2012)

29. S. Dong, W.Z. Zhang, P. Hu et al., Nitrogen content dependent microwave absorption property of nitrogen-doped SiC materials annealed in N_2: opposing trends for microparticles and whiskers. J. Alloys Compd. **758**, 256–267 (2018)

30. B.B. Li, B.X. Mao, T. He et al., Preparation and microwave absorption properties of double-layer hollow reticulated SiC foam. ACS Appl. Electron. Mater. **10**, 2140–2149 (2019)

31. J.L. Kuang, W.B. Cao, Silicon carbide whiskers: preparation and high dielectric permittivity. J. Am. Ceram. Soc. **96**, 2877–2880 (2013)

32. J.L. Kuang, W.B. Cao, Stacking faults induced high dielectric permittivity of SiC wires. Appl. Phys. Lett. **11**, 112906 (2013)

33. J.L. Kuang, P. Jiang, X.J. Hou et al., Dielectric permittivity and microwave absorption properties of SiC whiskers with different lengths. Solid State Sci. **91**, 73–76 (2019)

34. J.L. Kuang, T. Xiao, Q.F. Zheng et al., Dielectric permittivity and microwave absorption properties of transition metal Ni and Mn doped SiC nanowires. Ceram. Int. **46**, 12996–13002 (2020)

35. C. Grosse, A program for the fitting of Debye, Cole-Cole, Cole-Davidson, and Havriliak–Negami dispersions to dielectric data. J. Colloid Interface Sci. **419**, 102–106 (2014)